Boreal summer intraseasonal variability in coupled seasonal hindcasts

PRINCE K. XAVIER[1], JEAN-PHILIPPE DUVEL[1] AND FRANCISCO J. DOBLAS-REYES[2]

[1]*Laboratoire de Meteorologie Dynamique, Ecole Normale Superieure, Paris, France*

[2]*European Centre for Medium-Range Weather Forecasting, Reading, UK*

Submitted to Journal of Climate

Submitted August 2007

Revised December 2007

Corresponding author address:

Jean-Philippe Duvel, Laboratoire de Meteorologie Dynamique, Ecole Normale Superieure, 24 Rue Lhomond, 75231 Paris, France. E-mail: jpduvel@lmd.ens.fr

ABSTRACT

The intraseasonal variability (ISV) associated with the Asian summer monsoon represented in seven coupled general circulation models (CGCMs) as part of the European DEMETER project is analyzed and evaluated against observations. The focus is on the spatial and seasonal variations of ISV of outgoing long wave radiation (OLR). The large-scale organization of convection, the propagation characteristics and the air-sea coupling related to the monsoon ISV are also evaluated. A multi-variate Local Mode Analysis (LMA) reveals that most models produce less organized convection and ISV events of shorter duration than the observed. Compared to the real atmosphere, these simulated patterns of perturbations are poorly reproducible from one event to the other. Most models simulate too weak sea surface temperature (SST) perturbations and systematic phase quadrature between OLR, surface winds and SST, indicative of a slab-ocean-like response of the SST to surface flux perturbations. The relatively coarse vertical resolution of the different ocean GCMs (OGCMs) limits their ability to represent intraseasonal processes, such as warm layer formation, which are important for realistic simulation of the SST perturbations at intraseasonal time-scales. Models with the same atmospheric GCM (AGCM) and different OGCMs tend to have similar biases of the simulated ISV indicating the dominant role of atmospheric models in fixing the nature of the intraseasonal variability. It is, therefore, implied that improvements in the representation of ISV in coupled models have to fundamentally arise from fixing problems in the large-scale organization of convection in AGCMs.

1. Introduction

A large volume of research in the last few decades examined the potentials of dynamical models in predicting the seasonal mean rainfall of Asian summer monsoon. Due to the intrinsic predictability limits in the system (e.g. Goswami 1998) and the model biases (Gadgil and Sajani 1998), none of the present day GCMs has shown useful skill for seasonal predictions of monsoon rainfall (e.g. Wang et al. 2005). Considering the evidence (Goswami and Ajayamohan 2001) that the seasonal mean monsoon is closely linked to the structure and amplitudes of intraseasonal variability (ISV, 20 to 90 days; see Goswami (2005) for a review), at least some part of the shortcomings in the seasonal forecasts could arise due to the biases in representing the intraseasonal modes. In recent years there has been increased need for the prediction of intraseasonal spells that can directly benefit farmers and hydrologists (Webster and Hoyos 2004; Xavier and Goswami 2007). Many studies have shown some potential for predicting the intraseasonal spells a few weeks in advance (Goswami and Xavier 2003; Waliser et al. 2003b). However, the performance of dynamical models are far below the empirical methods (Lo and Hendon 2000). Improvements of forecasts at extended range and seasonal time scales, to some extent, depend on the ability of current GCMs to represent ISV.

ISV is a difficult phenomenon to reproduce in the current GCMs as some studies have revealed. ISV in 15 AGCMs participated in the Atmospheric Model Intercomparion Project (AMIP) was examined by Slingo et al. (1996) and found that most atmospheric GCMs have large biases in accurately simulating the Madden Julian Oscillations (MJO, Madden and Julian (1994)) in terms of strength, propagation speed, seasonality and interannual variability. Basic states errors in the models including the annual cycle and basic relationships between warm sea surface temperatures (SST) and precipitation rate are also related to quality of the MJO simulations. Sperber et al. (2001) evaluated the link between intraseasonal and interannual variability in 7 AGCMs forced with observed monthly SST as part of the Seasonal Prediction Model Inter-comparison Project (SMIP). Even though most models simulated the dominant mode of ISV, the relationship to seasonal means was poorly reproduced. In another study, the

ISV of the Asian summer monsoon was analyzed by Waliser et al. (2003a) using data from 10 AGCMs participating in the CLIVAR/Asian-Australian Monsoon Panel. The results showed that the ability of a model to represent ISV in summer and winter are strongly linked. The model ISV was found to be less coherent, lacked sufficient eastward propagation, reduced zonal and meridional spatial scales than the observed ISV and was often limited to either one or the other side of the maritime continent. Some of these biases point to the limitations in parameterizing the convection in AGCMs.

Many recent studies show that the intraseasonal variations in cloudiness and surface winds produce significantly strong perturbations of the SST (Bhat et al. 2001; Sengupta and Ravichandran 2001; Vecchi and Harrison 2002; Webster et al. 2002) which can feed back to the atmosphere in triggering convection. Over most regions, these intraseasonal SST variations are mainly a result of ISV of surface heat fluxes, dominated by the latent heat flux and incoming shortwave components. Over such regions, a 1/4 phase difference between the minimum of convection and the maximum SST is expected. In addition to the ISV of surface fluxes, the depth of the ocean mixed layer is an important factor that determines at the same time the reactivity and heat content of the upper ocean layer (Bellenger and Duvel 2007; Maloney and Sobel 2004). The variation of the temperature of the ocean mixed layer is due in part to fluctuations of the net heat flux at the surface caused by intraseasonal perturbations of cloudiness and surface winds. Other physical sources may however also contribute to the ISV of mixed layer temperature, such as the mixing with deeper layers caused by the deepening of the mixed layer (Duvel et al. 2004; Duvel and Vialard 2007). In addition, the formation of surface warm layers increase the SST during low-wind phases of the intraseasonal events, contributing to amplify the amplitude of the intraseasonal perturbation of the SST. This strong air-sea coupled nature of the ISV was, obviously, not taken into account in the AGCMs considered above and may be a major cause of the poor representation of ISV in these studies. Therefore, the simulation of ISV needs to be assessed in coupled GCMs. Such coupled integrations are expected to produce more realistic intraseasonal amplitude, propagation characteristics and phase re-

lationship between atmospheric and oceanic parameters (Fu et al. 2003; Kemball-Cook et al. 2002). Improvements resulting from the coupling with the ocean in turn may result in improved predictability of the ISV (Fu et al. 2006).

Even though the importance of air-sea coupling in the ISV simulations is recognized, a systematic approach to the ISV evaluation in current CGCMs is not available. The objective of this study is to perform a comprehensive evaluation of the representation of ISV in a set of multi-model coupled simulations. DEMETER (see Section 2) multi-model seasonal hindcasts are used for this purpose. This study focuses on the seasonality and the air-sea processes associated with the ISV using a new approach to characterize the intermittent organized convective perturbations. It is based on the Local Mode Analysis (LMA) introduced by Goulet and Duvel (2000) and further developed as a multivariate approach by Duvel and Vialard (2007). This multivariate approach is used here to extract SST and surface wind speed (SWS) perturbations related specifically to large-scale organized convective perturbations. An objective assessment of the model biases in representing the ISV and their possible causes could help to rectify them and improve the simulations. In addition, the assessment of ISV in seasonal hindcasts (see Section 2) is a well-suited approach to study the relationship between the ISV and monthly and seasonal predictability. Our future research will be focusing on understanding this link.

Section 2 presents the details of DEMETER hindcasts and Section 3 describes the LMA approach used to extract the large scale organized convective events and the associated variability in SST and SWS. The model assessment in terms of the climatological 20-90 days intraseasonal variance and their seasonal evolution for the NH summer hindcasts is presented in Section 5. Section 6 evaluates the ISV in the hindcasts using the multivariate LMA. A detailed comparison of the periods, degree of organization and the reproducibility of the intraseasonal modes in the models against the observations is also given. In order to analyze the role of the coupling in the representation of the ISV, a particular emphasis is given on the phase relationships between OLR, SST and SWS (Section 7). The role of AGCM in determining the properties of ISV is discussed in Section 8. Summary and discussions are given in Section 9.

2. Models and data sets

DEMETER is the acronym of the European project entitled 'Development of a European Multi-model Ensemble system for seasonal to inTERannual prediction' (Palmer et al. 2004). It consists of a suite of 7 coupled European GCMs whose components are given in Table.1. For each model (except for SMPI) uncertainties in the initial conditions are represented through an ensemble of nine different ocean initial conditions. This is achieved by creating three different ocean analyses; a control ocean analysis forced with momentum, heat and mass flux from the ECMWF Reanalysis (ERA40) and two perturbed ocean analyses created by adding wind stress perturbations to the ERA40 momentum fluxes. The wind stress perturbations are randomly taken from a set of monthly differences between two quasi-independent analyses. In addition, in order to represent the uncertainties in SSTs, four SST perturbations are added and subtracted at the start of the hindcasts. The atmospheric and land surface initial conditions are taken from the ERA40 data set. A separate coupled initialization method has been used for SMPI. It uses the ocean and atmosphere initial conditions from a coupled simulation with a strong relaxation to observed SSTs. This implies that there was no actual atmospheric information from an analysis in the initial conditions. The ensemble was generated by starting each member from a lagged initial date, from eight days before the start date of the hindcast. SCNR did not use atmospheric analysis to initialize its hindcasts. Instead, atmospheric and soil initial conditions were taken from an AMIP-type integration with ECHAM4. Ocean observations have been assimilated only in the UKMO run after 1987. The DEMETER hindcasts starts from 1 February, 1 May, 1 August or 1 November. Each hindcast is an ensemble of nine integrations (nine members) of six months. All seven models have been run for a common period of 1980-2001, although some models have been integrated over an even longer period (1958-2001). In this study, the common period 1980-2001 is used in order to facilitate comparison between models.

CNRM and CRFC uses the same AGCM (ARPEGE) and so do LODY and SCWC (ECMWF IFS), but with different Ocean GCMs (OGCMs). OPA version 8.1 is coupled with ARPEGE

and ECHAM4 in the CNRM and SCNR respectively. Version 8.2 of OPA is common for CRFC and LODY. These pairs of models may be used to account for the relative importance of the atmospheric or oceanic processes crucial for the ISV simulation.

This study uses OLR (a reliable observable quantity used as a proxy for deep convection), and the associated variability in SWS (at 10 m) and SST in the hindcasts starting from 1 May. These model variables are compared with NOAA interpolated OLR (Liebmann and Smith 1996) and surface winds and SST from ERA-40 reanalysis. SST data provided by ERA-40 (same as Reynolds and Smith (1994)) is weekly averaged data. It is a blend of satellite estimates with ship and buoy reports and is known to capture the cooling early in the monsoon season at the Bay of Bengal and SST changes in late summer, but not the ISV during July and August (Sengupta and Ravichandran 2001). This is because the satellite infra-red radiation sensors are not capable of measuring surface parameters in the presence of clouds and in situ data is sparse. Since November 1997 the National Aeronautics and Space Administration (NASA) Tropical Rain Measuring Mission (TRMM) Microwave Imager (TMI) has provided an unprecedented view of the tropical SST variability even in the presence of clouds (Wentz et al. 2000). SST ISV in Reynolds and Smith (1994) is known to be less than half of that from TMI for certain regions and seasons (Duvel and Vialard 2007) despite their similarity in the spatial patterns of variability. However, with the caution on the reported underestimation of the amplitude of intraseasonal SST fluctuations (Duvel and Vialard 2007), we use this data set to compare with the hindcasts, as this is the only available SST dataset that spans the hindcast period considered. The maximum intraseasonal variance of convection in summer is located over the Indian Ocean (Duvel and Vialard 2007). To focus on the ISV over Indian Ocean LMA is performed over the Indian Ocean basin (40°-110°E, 20°S-30°N).

3. The local mode analysis (LMA)

Spatial patterns and temporal characteristics of the intraseasonal convective events are determined using the local mode analysis (Goulet and Duvel 2000). The LMA makes it possible

to detect and characterize in a simple mathematical form the main events of an intermittent phenomenon that succeed one another in time. It gives a pattern for each intraseasonal event, that allows us to compare the characteristics of different events in models and observations. A full description of the approach is given in Duvel and Vialard (2007). Here we give a brief account of the main features of LMA.

The LMA technique is based on a CEOF computation on a running time section (of 90 days here). For each time step m of the running analysis only the first CEOF is retained which corresponds to one particular temporal spectrum $\widetilde{\psi}_p^m(k)$ and a spatial pattern $\widetilde{Z}_p^m(x)$ and explaining a percentage of variance Π_p^m. p is the parameter considered (OLR here), k is the temporal harmonic and x is the region. Maxima in the Π_p^m time series are then identified and the first CEOF of the corresponding time section are called the *Local Modes*. This local mode is assigned with the date of centre of the 90-days window. One can demonstrate that the spatial patterns $\widetilde{Z}_p^m(x)$ of these *Local Modes* (or organized convective events) are more persistent in time and more spatially coherent than the patterns in their neighborhood (Goulet and Duvel 2000).

For a grid point x of the parameter p, the reconstructed time series associated with the local mode of the time step (m) is given by:

$$S_p^m(x,t) = A_p^m(x) B^m(t) \cos\left(\phi_p^m(x) + \chi^m(t)\right) \tag{1}$$

where $A_p^m(x) = \left|\tilde{Z}_p^m(x)\right|$ and $\phi_p^m(x) = \arg[\tilde{Z}_p^m(x)]$ are respectively the regional standard deviation and phase of the leading complex eigenvector $\tilde{Z}_p^m(x)$. $B^m(t)$ and $\chi^m(t)$ represent respectively the amplitude and phase of the first CEOF of the time section m.

This technique may be further used to study the perturbations of a second parameter, q associated with the perturbation of the leading parameter p. Indeed, the projection of the normalized spectrum $\tilde{\psi}_p^m(k)$ done on the Fourier coefficient of another parameter q give a $\tilde{Z}_{p,q}^m(x)$ that represents the spatial pattern of the perturbation of q related to the large scale

organized perturbation of p, through a "spectral key" $\tilde{\psi}_p^m(k)$. In other words, the distribution of amplitudes and phases of $\tilde{Z}_{p,q}^m(x)$ represents the part of the regional signal of q that is correlated with the large-scale organized perturbation of p represented by the Local Mode m.

Following the method detailed in Duvel and Vialard (2007), it is possible to compute then the corresponding average patterns for other parameters. These patterns are used in this study to analyse the average relationship between the OLR, SST and the surface winds intraseasonal perturbations. The LMA makes it also possible to measure the resemblance between an average pattern and the patterns of each event. This is very important to verify if this average pattern is only a mathematical object or if it is representative of the different events, i.e., if it is appropriate to give a physical interpretation of the phenomena. As in Goulet and Duvel (2000), this resemblance is computed as a normalized distance between the complex eigenvectors representing the average pattern and the pattern of each Local Mode. A normalized distance of 0 means that the patterns are identical and a normalized distance 1 means that the two patterns are orthogonal.

4. Seasonal migration of the intertropical convergence zone (ITCZ)

There are large seasonal variations over the Indian monsoon region between May and September. This has an impact on the seasonal distribution of the location of the main convective intraseasonal events. The intraseasonal perturbations during summer are characterized by a northward migration of the ITCZ from south of Equator to about 25°N. A number of pre-monsoon convective events over south Bay of Bengal in May are associated with this seasonal transition and the onset of the Indian monsoon with strong amplitude in the Arabian Sea occurs generally in June (Bellenger and Duvel 2007). This gives significant differences in the seasonal variations between the Arabian Sea and the Bay of Bengal as also highlighted in Duvel and Vialard (2007). The skill of the models in representing these seasonal variations of the monsoon is described here (Fig.1).

A common problem for most models is the lack of migration of the ITCZ up to 25°N as in the observations. SCWC and LODY do not exhibit any significant seasonal variations over the Bay of Bengal, with a narrow ITCZ that establishes around 10°N at the beginning of June and persists during the season. This indicates that the intraseasonal convective fluctuations will be restricted in this narrow region of convective activity. On the other hand, SMPI has an exaggerated double ITCZ, with hardly any northward propagation from the southern to the northern ITCZ. UKMO, CNRM and CRFC have low OLR values north of 25°N with a quite realistic northward shift around end of June. The seasonal cycle of OLR also has influence on the character of ISV embedded on them and is a main focus of this study.

Models which share the same AGCM tend to have almost identical behavior in representing the seasonal cycle and character of ISV. For example, CRFC and SCWC represent the properties of CNRM and LODY respectively. Therefore, only a representative of the models with the same AGCM will be presented in the following sections. Possible reasons for this behavior is discussed in Section 8.

5. Intraseasonal variance

The major features of the ISV (defined here as the standard deviation of 20-90 days filtered anomalies) of OLR, SWS and SST and their seasonal variations related to the seasonal variations of the ocean mixed layer is presented here. A brief description of the construction of intraseasonal anomalies is needed since it is not trivial to define ISV at the beginning of the hindcasts using filters unless some past data is prefixed to the hindcasts. For most models ERA40 data can be used for this purpose since the initial conditions are taken from ERA40. However, SCNR and SMPI do not initialize their atmospheric component with ERA40 data, but with a data from a simulation. Since we are using a Lanczos filter (Duchon 1979) with 91 weights, at least 45 days of past data from the specific experiments that are used to generate initial conditions (see Table.1) would be needed to be pasted at the beginning of the hindcasts. Since these data are not available, we alternatively use daily ERA40 anomalies of each year

(constructed by removing the daily climatological values based on 21 years, Fig.2a) prefixed to the anomalies of the hindcasts (constructed by removing the daily model climatology). A 20-90 days band pass Lanczos filter with 91 weights is then applied on the combined (120 days of ERA40 anomalies and 180 days of hindcast anomalies) daily anomalies to extract the intraseasonal signal (Fig.2b). The removal of daily climatological values from the prefixed ERA40 data and the hindcasts avoids strong discontinuities between the ERA40 and the hindcasts results due to their different climatological states (Fig.2a). The differences in the methods of initialization could impart some differences in the models' ISV behaviour. However, It may be noted that the influence of the initialization is carried only up to 15-20 days maximum. This is referred to as the deterministic limit of predictability. Beyond that the model ISV arises from the coupled interactions between convection, dynamics and ocean surface. Since the hindcasts are initialized at 1 May, there may be some influence on the ISV events those occurring in the first half of May (though this number is not large). However, the initialization is not expected to impact much to the ISV occurring from June through September.

The seasonal variations of ISV is intimately linked to the seasonal march of the monsoon (Bellenger and Duvel 2007). A comparison of the amplitude and seasonality of intraseasonal variability of OLR and SWS in the models with the observations is given in Fig.3. An important feature of the observed ISV of OLR among those detailed in Duvel and Vialard (2007) is the strong convective fluctuations (analogous to the large OLR ISV amplitude) over the Bay of Bengal and the eastern Indian Ocean in May associated with the commencement of the northward propagation of the ITCZ and the low level wind flow across the southern parts of India resulting in heavy rainfall. These pre-monsoon events has been referred to as bogus onset, Flatau et al. (2001) (Fig.3). June is shown separately which corresponds to the actual monsoon onset and JAS for which the ISV amplitude is smaller over north Indian Ocean. With the progression of the season, the largest convective intraseasonal variability is observed in June over the Arabian Sea (Fig.3), with corresponding surface wind perturbations. Two secondary maxima of OLR amplitude are found, one over the east equatorial Indian Ocean and another

over the northern Bay of Bengal. Sudden strengthening of convective perturbations and surface winds at the time of the monsoon onset causes a progressive deepening of the mixed layer in both the Arabian Sea and Bay of Bengal (Fig.5) for the rest of the season. The ocean thermal conditions are essentially controlled by the ocean mixed layer depth (MLD), with a shallow mixed layer producing large SST variability when the heat fluxes are dominant. As a result, the largest SST variability is more confined to upwelling regions and to the northern Bay of Bengal and Arabian Sea where the MLD remains shallow (Fig.4).

In all the models, largest biases are seen in representing the amplitudes and locations of the OLR ISV, particularly the maximum over the Bay of Bengal in May and over Arabian Sea in June are not well reproduced (Fig.3). There is a general tendency of most models to produce unrealistically large OLR variability over the Western Indian Ocean. Abrupt transition of convective perturbations to the Arabian Sea during June is reproduced in few models (SCNR, SCWC/LODY) to some extent, despite biases in the amplitudes. However, there sudden increase of SWS over Arabian Sea in June is reproduced only in CNRM and SCNR. The progressive weakening of the ISV amplitudes from May to September is rather well represented in all models despite their intrinsic biases in amplitudes and locations of ISV. It may be noted from Fig.5, that during May, MLD are quite shallow over the Indian Ocean basin, (SCWC generally produce deeper mixed layers) making the ocean surface layer highly reactive to the surface fluxes. All models except SCNR show a progressive deepening of mixed layer with the season. As a result, the reactivity of the ocean models to the atmospheric fluxes are limited to the regions of shallow mixed layer regions such as the northern Arabian Sea and the Bay of Bengal (Fig.4). An important point to be noted here is the suppressed amplitudes of SST ISV in the models (and Reynolds SST) compared to the TMI. Models produce only about 20% of the observed SST amplitudes. The possible reasons of this strong SST bias will be discussed in Section 7.

6. Seasonality of organized ISV

While LMA provides a wealth of information on the characteristics of organized ISV as mentioned above, in this section we focus on the seasonality in the organization of the modes, average propagation characteristics and the air-sea interactions associated with large-scale organized perturbations of the convection. To demonstrate the seasonality in the character of organized ISV, average modes of OLR for May, June and July-September (JAS) are constructed (Fig.6).

Maximum amplitude of observed organized perturbations of convection over the south Bay of Bengal happens in May (Fig.6, top panels) with a northward propagation speed of about 2°/day, superimposed on a slightly faster eastward propagating perturbation. In June, the most striking difference compared to May is the strong perturbation of convection between 10-25°N over the eastern Arabian Sea (Fig.6). This dramatic shift in the patterns is characteristic of the monsoon onset, with clear northward propagation of convective perturbations from eastern Equatorial Indian Ocean.

Fig.6 compares the model behavior in describing the large scale organization and the seasonal variations of the convective ISV events. A clear shift of active convection centers to the Arabian Sea and Indian subcontinent from May to June is represented only in CRFC/CNRM and SCWC/LODY to some extent. A problem for CRFC and SCWC is the presence of westward propagation. UKMO produces eastward north-eastward propagation in May and June but slower westward propagating signals spanning the equator during JAS, indicating Rossby wave propagations. This reveals the poor consistency of modes in this model. The power spectrum of OLR over the Bay of Bengal reveals that (not shown) some models have more power in the synoptic (2-10 days, in CRFC/CNRM) and 10-20 day band (in UKMO) than the observations. Extension of these shorter period-westward propagating perturbations (Krishnamurti and Bhalme 1976) into the intraseasonal band may explain the westward propagating ISV in these models. If one considers only the propagations of organized intraseasonal convection perturbations, SCNR and CRFC/CNRM are better than the rest of the models due to

their large-scale organization and northeastward propagation from the western Indian Ocean. The amplitude and location of ISV in JAS is represented in SCNR relatively well. However, SCNR has a dominant eastward propagation that explains why the convection does not reach the northern Bay of Bengal in this model, despite having a better spatial organization and reasonable amplitude of convective perturbation.

Thanks to the LMA, contribution of the organized convective perturbations to the local ISV amplitude (amplitude of 20-90 day filtered time series) is examined here (Fig.7). For each event (the local mode signal), the regional variance percentage is the ratio of the amplitude of the organized convective events to the amplitude of 20-90 days filtered OLR (Fig.3). The larger this ratio, the larger the contribution of the large-scale organized convection to the local variability of convection. In the observations, the regions for which the organized OLR perturbation has the larger impact are the East equatorial Indian Ocean and East Arabian Sea. For these regions, the large-scale organized convective events contribute more than 60% of the local ISV. The difference between observed and modeled variance percentage is quite large (Fig.7). High values over the Arabian Sea are detectable for nearly all models, but with smaller variance percentage. The variance percentage over the East equatorial Indian Ocean region remains also very small for all models. It suggests that the models tend to generate ISV over various locations, while in the observation, the convective perturbations are better organized with a reproducible pattern (see also Fig.8c). In the models the variance percentage is quite small compared to the observed modes (Fig.7) despite having reasonable amplitudes of total ISV (Fig.3). This ISV is thus linked more to local convective events not well organized over the basin. Therefore it is important to understand the behavior of the organized convective events to be able to interpret their contribution to the total ISV of the season.

Since the organized events have characteristic differences following the march of the summer season in observations and hindcasts, it is expected that the properties which define these organized events such as their periods, degree of organization and reproducibility of the patterns also have similar seasonal variations (Fig.8). Here the degree of organization is defined

as the percentage of variance explained by the first CEOF and the reproducibility of the modes are described by the distance (see Section 3) between the pattern of each individual event and their average summer pattern. The parameters shown in Fig.8 result from the average over 21 years in the case of observations and all the 21 years and 9 members for the hindcasts.

There is a rather steady decrease of periodicity from May that is well depicted by the models (Fig.8a). The models, however, tend to underestimate the periodicity, except for some models in June and July. The observed percentage of variance is clearly above all the models during May to August with very large values in May related to the pre-monsoon convective events (Fig.8b). The (average) long periods and large increase of variance percentages of the events from April to May and June in observations are evidences of interannually recurring organized monsoon onset. It is therefore implied that these results could have some relevance on the interannual predictability of the monsoon onset. All models produce an increase of variance percentage in June, but smaller than observed. This indicates that either there are no pre-monsoon events in any of the models or the monsoon onsets are generally happening in June. For these two parameters, values in March and April are purely arising from the ERA40 OLR anomalies, but influenced weakly by the hindcasts at one end of the 90 days window.

The distance of each individual event from the average May-September pattern is computed and averaged for each month (Fig.8c). An intriguing feature in the observations is the event to event consistency revealing the similarity of each individual event to the average event of the season. The large seasonal variations in the observations indicate the events in spring and autumn are characteristically (phase and amplitude distributions) different from the average summer pattern. The patterns of individual events in models are far from their average summer ISV pattern with no model having a monthly average distance less than 0.5. The observed and modeled distribution of the distances in summer (May-September) to their average summer pattern is shown in Fig.9. The maximum observed distances are at 0.2 and 0.3 (almost 50% of the events), but with a small fraction of close to orthogonal patterns. The distances of patterns in models are rather large with peaks between 0.4 to 0.7. The large spread of distances

suggest, in addition to the poor correspondence between each individual event and its average pattern, the consistency among events in the models are poor. SCNR produces slightly better reproducibility compared to other models. The unique capability of LMA to measure these distances help us to reach the conclusion that average patterns of events in the models (Fig.6) are more of mathematical objects contributed by poorly organized events that differ significantly from each other, rather than a meaningful representation of real physical phenomena as in the observations. Therefore, this analysis cautions the interpretation of seasonal average patterns as physical modes in models presented here.

In addition, a more specific approach to measure the ability of models to reproduce realistic patterns is presented in Fig.10. The distance of each individual event in the models are compared to the average observed pattern of May, June, JAS and the May-September. The distance of each observed event to the average observed pattern is also given for comparison. Notably, the observed distances are skewed towards 0 while the model distances are skewed towards 1. The observed patterns in May and June (related to the monsoon onset) are highly reproducible, but distance of the patterns in the models to the observed pattern in these two months are quite large, especially for UKMO and SMPI. This demonstrates that the pattern of the onset event in the models are far from the observations. Considering the entire summer season, the large errors of patterns in UKMO and SMPI arise mainly from their poor representation in May and June. Among these models SCNR stands out, particularly in its representation of JAS patterns.

7. Air-sea interactions

The observed ISV of convection is maximal over the warm oceanic regions around the Indian subcontinent (with relative minimum over the subcontinent, Fig.3), suggesting the role of air-sea interactions in the organization of convection at intraseasonal time scales. The ISV of SST is strong in the northern Bay of Bengal and Arabian coast (Fig.4) and the surface wind perturbations also have maxima over these two regions. The coherent evolution of OLR, SST and surface wind perturbations and the quadrature relationship of SST with OLR and

surface winds indicates that the intraseasonal SST fluctuations are essentially driven by the atmospheric ISV through the net heat flux (Q_{net}) at the surface and mixing with deep waters due to surface stress, with the latent heating (proportional to SWS) and the insolation (proportional to OLR) being two major contributing terms of Q_{net} over the Bay of Bengal. However, the quadrature relationship between SST and Q_{net} is not found to hold good over the equatorial Indian Ocean and the western Indian Ocean coastal region (Sengupta et al. 2001) where the ocean dynamics also seem to play a role in determining the SST (Duvel and Vialard 2007). Waliser et al. (2004) studied the response of the Indo-Pacific ocean to the atmospheric ISV forcing by using an OGCM forced by canonical atmospheric ISV conditions constructed from the observations. While Q_{net} associated with the ISV is the major forcing, they found that the mixed layer variations tended to contribute positively to SST variations. Further, contributions from advection and or/entrainment within the Somali Current region and equatorial Indian Ocean are significant.

Using the multivariate LMA approach (Duvel and Vialard 2007), it is also possible to compute the SST and surface wind perturbations associated to the large scale organized convective perturbations (see Section 33). It is also possible to obtain the patterns for the average response of SST and surface winds to large-scale organized intraseasonal OLR perturbations. The average phase relationships between the OLR, SST and SWS (Fig.11) can explain some of the air-sea interaction processes in this region. In observations, the quadrature relationship between SST and OLR holds good over some regions, for which the atmospheric heat fluxes are the dominant factor for mixed layer temperature and SST variability and OLR out of phase with SWS. For other regions, processes such as the warm layer formation, mixing with deep water due to the surface wind stress or upwelling could influence the variations in SST. Only SCNR despite its low amplitude of SST, has some fidelity in simulating these features, while most models indicate a nearly perfect quadrature relationship between SST and OLR over the Bay of Bengal and eastern Indian Ocean (Fig.11, CRFC is shown as an example for the other model with similar behavior).

As already documented in (Duvel and Vialard 2007), the phase relationship between winds and SST due to other processes is however more variable with respect to this 1/4 lag of period related to the simple integration of surface fluxes by a mixed layer of nearly constant depth. For example, in the presence of a warm layer, prior to the convective perturbation, the daily mean SST will tend to be maximal for the minimum wind and will sharply decrease towards the average mixed layer temperature as soon as the winds rise above a certain threshold. Even if the mixed layer temperature then evolves under the influence of surface flux forcing, the phase relationship between SST and winds will be modified by this warm layer formation and destruction with the SST becoming more in phase opposition with the surface winds. A similar behavior is expected for a rapid deepening of the mixed layer due to wind bursts that produce a fast cooling related to the mixing with deeper and colder waters. This nearly 1/8 phase difference between SST and winds are reproduced to some extent only in SCNR with the covariability nearly over the same regions.

A detailed diagnosis on the phase lags between SST, OLR and SWS is presented in Fig.12. The distribution of the phase differences between these three parameters over the Bay of Bengal is constructed. This is a region for which processes other than the surface heat fluxes also play role in determining the SST. This region shows large differences between observations and models in the mutual phase relationships between these variables (Fig.11). A large number of values of observed SST-OLR phase differences are between 1/4 and 1/2. As seen from the average phases in Fig.11, all models (except SCNR) produce a strong tendency for phase quadrature between SST and OLR (Fig.12a). Larger differences between observations and models are found for the phase differences of SST-SWS and OLR-SWS (Fig.12b,c). While the observed SST is nearly out of phase with the surface winds, this relationship is also very systematically represented in the models with nearly a phase quadrature between maximum wind and maximum SST (Fig.12b). Some of these too systematic behavior of the models appears to be related to the relationship between convection and dynamics in the models. This is substantiated by the OLR-SWS phase difference (Fig.12c) which shows the tendency of all

models to produce nearly in phase relationship between convection and surface winds, while in reality it is much more variable.

To simplify the above discussion, a generalized schematic is presented in Fig.13 based on the maximum frequencies of phase differences in Fig.12. A major difference between the observations and models in terms of the evolution of ISV is the differences in the OLR-SWS phase relationship. The nearly in phase relation between maximum convection (minimum OLR) and maximum SWS in the models is indicative of the systematically fast response of surface winds to convection, unlike in the observations. Contrary to the very similar behavior of all models (except SCNR) in representing SST-OLR phase relationship (Fig.12a), OLR-SWS relation is more variable among different models (but almost identical for models with same AGCM, Fig.12c). This highlights the issues in the boundary layer and convection parameterizations in the models. The better SST-OLR phase relationship in SCNR (Fig.12a) may partially be attributed to its improved OLR-SWS relationship that contributes to a better phase relationship between SST and SWS (Fig.12b) as well. A first order explanation for this behavior may be that in all the other models incoming shortwave flux may be dominant over the latent and sensible fluxes, while SCNR is able to produce quite realistic latent heat fluxes due to its stronger surface wind perturbations (Fig.3b), which together with the shortwave flux could lead to a shorter delay between SST and OLR as in the observations.

8. Role of atmospheric processes in model ISV

Most of the results presented above did not explicitly show the behavior of the models that share the same AGCM since their properties on the intraseasonal variations of both atmospheric and oceanic parameters are almost identical. A set of comparisons of the OLR and SST ISV among three models (CRFC, LODY and SCWC) are shown here (Fig.14). While CRFC and LODY share the same OGCM (OPA 8.2), apart from the obvious differences in simulating the ISV of OLR, significant differences in the amplitudes of SST ISV is also seen (Fig.14c). On the contrary, LODY and SCWC with the same AGCM (IFS) and very different OGCMs (OPA8.2

and HOPE-E), produce almost no differences in the OLR ISV (Fig.14b). The differences in SST ISV are also very small over the highly reactive regions of the northern Indian Ocean. The small differences seen over the equatorial Indian ocean between these models are related to the differences in the horizontal resolution of the equatorial wave guide (Fig.14d). However this difference is rather small compared to that of Fig.14c.

Guilyardi et al. (2004) presented evidence on the dominant role of atmospheric component in setting El Nino properties (periodicity and amplitude) in coupled GCMs mainly due to parameterization of the surface boundary layer and convective processes that alter the coupling strength, thus reducing the atmospheric sensitivity to SST changes. In addition, horizontal resolution of the AGCMs also influence the coupling. At intraseasonal time scales, the biases in defining the oceanic mixed layer also can have some impact on the coupling. How well the SST is simulated and how effectively they feed back to the atmosphere and interact with convection will depend on the boundary layer and convective parameterizations also. However with the present understanding of the phenomenon, these ocean to atmosphere feedbacks are not clearly resolved. Therefore in the present day coupled models, the improvements in the simulation of the coupled behavior of ISV has to be fundamentally arise from the atmospheric models. In addition, right amplitudes of diurnal SST variations are shown to be important for representing the right SST ISV amplitudes (Bernie et al. 2007). Current climate models, however, are not configured to resolve the diurnal cycle in the upper ocean or the interaction of the ocean and atmosphere on these time scales. Ocean GCMs with high enough vertical resolution to resolve the diurnal warm layers at the surface and the exchange of heat at the bottom of the mixed layer will be needed to address this issue.

9. Summary and discussions

Tropical summer intraseasonal perturbations are highly intermittent with a strong seasonal variability. As a consequence, it is difficult to extract simple and significant diagnostics from averaged statistics of ISV. In addition, the physics of the phenomenon is still poorly understood.

In particular, the effect of the coupling between the perturbations of the deep convection and the dynamical response (or forcing if equatorial waves are supposed to be the driving mechanism) on the intraseasonal variability is not well established. This is even complicated by the possible influence of the coupling between the convective activity and the ocean surface temperature on the fluctuation of organized intraseasonal perturbation of the deep convection. The complexity of these interactions leads to real difficulties in representing these intraseasonal perturbations in forced or coupled atmospheric models. There is a poor representation of the mean state and of the average seasonal evolution of the monsoon circulations in the coupled models. This leads to (and is certainly also partly related to) a wrong representation of the intraseasonal variability of the deep convection and thus of the large-scale organization of the convective perturbations.

Because of these difficulties, the present analysis may be considered as a first attempt to assess the coupled character of the intraseasonal activity in CGCMs. To answer the above critical points, a particular attention was given to:

- The character of boreal summer intraseasonal activity when it is strongly linked to the seasonal march of the monsoon (see also Bellenger and Duvel (2007)).

- The intermittency of the phenomenon by considering distributions of the characteristics of the intraseasonal events rather than only average perturbation patterns (use of the multi-variate LMA).

- The evaluation of the representation of the coupling between the convection, the low-level wind and the SST at intraseasonal time scales.

A specific set of diagnostics was developed that aims to take into account these different points. Considering the ensemble of the DEMETER hindcast, we arrive at these preliminary conclusions. The multi-variate LMA shows that most models have problems in simulating large-scale organized intraseasonal perturbations of the convection. In addition, perturbation patterns are more variable from one intraseasonal event to another compared to observation

even for a limited basin. The well organized observed modes in May-June are almost reproducible from one year to another, whereas in the models, these onset patterns are much more variable. This chaotic behavior of the ISV in the models will have some impact on predicting the onset events. Some models do exhibit some form of north-eastward propagation of the perturbations over the Indian Ocean during boreal summer. Realistic periods of the modes (25-35 days) are produced in a few models, while others produce shorter periods (20-25 days). The contribution of organized modes to the total ISV in the models is rather poor compared to the observations. One possible source of deficiency in organizing intraseasonal large-scale convective perturbation could be the air-sea interaction.

Even though most models produce average SST variations of the order of 0.15 K over the north Bay of Bengal and Western Arabian Sea, this number is significantly less than the observed ISV of SST. These are the regions of shallow mixed layers and the ocean can respond rapidly to the surface fluxes. A comparison between the ISV of SST in the models and the TMI reveals that only about 20% of the observed ISV of SST over the Bay of Bengal is represented in the models.

There is a strong influence of the atmospheric forcing in driving the SST as indicated by the similarity in the SST amplitude and patterns of LODY and SCWC (with same AGCM, but different OGCMs). It has been shown that air-sea coupling can modify the structure of the intraseasonal variability (Fu et al. 2003; Kemball-Cook et al. 2002). However, even when coupled with different OGCMs (OPA version 8.1 and HOPE, Table 1), the basic properties of the IFS model remain almost identical. The small amplitudes of SST perturbations may be related to underestimated surface turbulent and radiative fluxes perturbations given by the atmospheric models. This limits the perturbation of the ocean mixed layer temperature and may also generate insufficient mixing between the mixed layer and the deeper ocean during strong surface wind phase. Though air-sea coupling is important for the models to reproduce observed propagation characteristics and phase relationships between the convection and SST, the basic characteristics of the coupled model could arise mainly from the AGCMs. Therefore,

there is a fundamental requirement that the atmospheric models produce realistic organization and propagation of convection. Note however that, the ocean models considered here might have certain limitations in simulating realistic SST variability for the following reasons. The formation of diurnal warm layer over the oceans in clear and calm conditions is important in the air-sea interactions at intraseasonal time scales. These warm layers could trigger large scale organized convective perturbation that later evolve at intraseasonal time scale. The models could not reproduce the diurnal cycle of SST and have thus no potential for simulating the diurnal cycle of SST because the ocean exchanges fields with the atmosphere only once a day. The considered OGCMs have a poor resolution at the top of the ocean (say 10 m at the best). So there could be uncertainties in the determination of the oceanic mixed layer, especially at the bottom of the mixed layer where the mixing with deeper and cooler waters could impact the heat budget of the mixed layer. Another factor may be the lack of representation of fresh water fluxes from the rivers into the north Bay of Bengal in the models, which can have significant impacts on the air-sea interactions (Sengupta and Ravichandran 2001) via the formation of a barrier layer. In order to address these issues, the coupled models will require the ocean component with high vertical resolution to resolve the surface warm layers and the bottom of the mixed layer. This, to a large extent, would contribute to the right intraseasonal SST amplitude and phasing with the convection by simulating the diurnal warm layers and the exchanges with deeper waters at the bottom of the mixed layer.

Acknowledgment. Interpolated OLR data is provided by the NOAA/OAR/ESRL PSD, Boulder, Colorado, USA, from their Web site at $http://www.cdc.noaa.gov/$. TMI SST data is obtained from $ftp.ssmi.com/tmi$. PKX and FJDR are supported by the European ENSEMBLES project.

REFERENCES

Bellenger, H. and J. P. Duvel, 2007: Intraseasonal convective perturbations related to the seasonal march of the Indo-Pacific monsoons. *J. Climate*, **20**, 2853–2863.

Bernie, D. J., E. Guilyardi, G. Madec, J. M. Slingo, and S. J. Woolnough, 2007: Impact of resolving the diurnal cycle in an oceanatmosphere GCM. Part 1: a diurnally forced OGCM. *Climate Dyn.*, **29**, 575–590.

Bhat, G. S., S. Gadgil, P. V. H. Kumar, S. R. Kalsi, P. Madhusoodanan, V. S. N. Murty, C. V. K. P. Rao, V. R. Babu, L. V. G. Rao, R. R. Rao, M. Ravichandran, K. G. Reddy, P. S. Rao, D. Sengupta, D. R. Sikka, J. Swain, and P. N. Vinayachandran, 2001: The Bay of Bengal monsoon experiment. *Bull. Amer. Meteor. Soc.*, **82**, 2217–2243.

de Boyer Montegut, C., G. Madec, A. S. Fischer, A. Lazar, and D. Iudicone, 2004: Mixed layer depth over the global ocean: An examination of profile data and a profile based climatology. *J. Geophys. Res.*, **109**, C12 003, doi:10.1029/2004JC002 378.

Duchon, C. E., 1979: Lanczos filtering in one and two dimensions. *J. Appl. Meteor.*, **18**, 1016–1022.

Duvel, J. P., R. Roca, and J. Vialard, 2004: Ocean mixed layer temperature variations induced by intraseasonal convective perturbations over the Indian Ocean. *J. Atmos. Sci.*, **61**, 1004–1023.

Duvel, J. P. and J. Vialard, 2007: Indo-Pacific sea surface temperature perturbations associated with intraseasonal oscillation of the tropical convection. *J. Climate*, **20**, 3056–3082.

Flatau, M., P. Flatau, and D. Rudnick, 2001: The dynamics of double monsoon onsets. *J. Climate*, **14**, 4130–4146.

Fu, X., B. Wang, T. Li, and J. McCreary, 2003: Coupling between northward propagating, intraseasonal oscillations and sea-surface temperature in the Indian Ocean. *J. Atmos. Sci.*, **60 (15)**, 1733–1753.

Fu, X., B. Wang, D. E. Waliser, and T. Li, 2006: Impact of atmosphere-ocean coupling on the predictability of monsoon intraseasonal oscillations (MISO). *J. Atmos. Sci.*, **64**, 157–174.

Gadgil, S. and S. Sajani, 1998: Monsoon precipitation in the AMIP runs. *Climate Dyn.*, **14**, 659–689.

Goswami, B. N., 1998: Interannual variations of Indian summer monsoon in a GCM: External conditions versus internal feedbacks. *J. Climate*, **11**, 501–522.

———, 2005: South Asian Monsoon. *Intraseasonal variability in the Atmosphere-Ocean climate system*, Lau, K. and D. Waliser, Eds., Praxis. Springer Berlin Heidelberg, 19–61.

Goswami, B. N. and R. S. Ajayamohan, 2001: Intraseasonal oscillations and interannual variability of the Indian summer monsoon. *J. Climate*, **14**, 1180–1198.

Goswami, B. N. and P. K. Xavier, 2003: Potential predictability and extended range prediction of Indian summer monsoon breaks. *Geophys. Res. Lett.*, **30(18) (1966)**, doi:10.1029/2003GL017 810.

Goulet, L. and J. P. Duvel, 2000: A new approach to detect and characterize intermittent atmospheric oscillations: Application to the intraseasonal oscillation. *J. Atmos. Sci.*, **57**, 2397–2416.

Guilyardi, E., S. Gualdi, J. Slingo, A. Navarra, P. Delecluse, J. Cole, G. Madec, M. Roberts, M. Latif, and L. Terray, 2004: Representing El Nino in coupled ocean-atmosphere GCMs: The dominant role of the atmospheric component. *J. Climate*, **17**, 4623–4629.

Kemball-Cook, S., B. Wang, and X. Fu, 2002: Simulation of the intraseasonal oscillation in the ECHAM-4 Model: The impact of coupling with an ocean model. *J. Atmos. Sci.*, **59**, 1433–1453.

Krishnamurti, T. N. and H. N. Bhalme, 1976: Oscillations of monsoon system. Part I: Observational aspects. *J. Atmos. Sci.*, **45**, 1937–1954.

Liebmann, B. and C. A. Smith, 1996: Description of a complete (interpolated) outgoing longwave radiation dataset. *Bull. Amer. Meteor. Soc.*, **77**, 1275–1277.

Lo, F. and H. H. Hendon, 2000: Empirical extended-range prediction of the Madden-Julian oscillation. *Mon. Wea. Rev.*, **128**, 2528–2543.

Madden, R. A. and P. R. Julian, 1994: Observations of the 40-50 day tropical oscillation: A review. *Mon. Wea. Rev.*, **122**, 813–837.

Maloney, E. D. and A. H. Sobel, 2004: Surface fluxes and ocean coupling in the tropical intraseasonal oscillation. *J. Climate*, **17**, 4368–4386.

Palmer, T. N., A. Alessandri, U. Anderson, P. Cantelaube, M. Davey, P. Delecluse, M. Deque, E. Diez, F. J. Doblas-Reyes, H. Feddersen, R. Graham, S. Gualdi, J.-F. Gurmy, R. Hagedorn, M. Hoshen, N. Keenlyside, M. Latif, A. Lazar, E. Maisonnave, V. Marletto, A. P. Morse, B. Orfila, P. Rogel, J.-M. Terres, and M. C. Thomson, 2004: Development of a European multimodel ensemble system for seasonal-to-interannual prediction (DEMETER). *Bull. Amer. Meteor. Soc.*, DOI: 10.1175/BAMS–85–6–853.

Reynolds, R. W. and T. M. Smith, 1994: Improved global sea surface temperature analyses using optimum interpolation. *J. Climate*, **7**, 929–948.

Sengupta, D., B. N. Goswami, and R. Senan, 2001: Coherent intraseasonal oscillations of ocean and atmosphere during the Asian summer monsoon. *Geophys. Res. Lett.*, **28 (21)**, 4127–4130.

Sengupta, D. and M. Ravichandran, 2001: Oscillations of Bay of Bengal sea surface temperature during the 1998 summer monsoon. *Geophys. Res. Lett.*, **28 (10)**, 2033–2036.

Slingo, J. M., K. R. Sperber, J. S. Boyle, J.-P. Ceron, M. Dix, B. Dugas, W. Ebisuzaki, J. Fyfe, D. Gregory, J.-F. Gueremy, J. Hack, A. Harzallah, P. Inness, A. Kitoh, W. K.-M. Lau, B. McAvaney, R. Madden, A. Matthews, T. N. Palmer, C.-K. Park, D. Randall, and

N. Renno, 1996: Intraseasonal oscillations in 15 atmospheric general circulation models: Results from an AMIP diagnostic subproject. *Climate Dyn.*, **12**, 325–357.

Sperber, K. R., C. Brankovic, M. Deque, C. Frederiksen, R. Graham, A. Kitoh, C. Kobayashi, T. Palmer, K. Puri, W. Tennant, and E. Volodin, 2001: Dynamical seasonal predictability of the Asian summer monsoon. *Mon. Wea. Rev.*, **129**, 2226–2248.

Vecchi, G. A. and D. Harrison, 2002: Monsoon breaks and subseasonal sea surface temperature variability in the Bay of Bengal. *J. Climate*, **15**, 1485–1493.

Waliser, D. E., K. Jin, I.-S. Kang, W. F. Stern, S. D. Schubert, M. L. C. Wu, K.-M. Lau, M.-I. Lee, V. Krishnamurthy, A. Kitoh, G. A. Meehl, V. Y. Galin, V. Satyan, S. K. Mandke, G. Wu, Y. Liu, and C.-K. Park, 2003a: AGCM simulations of intraseasonal variability associated with the Asian summer monsoon. *Climate Dyn.*, **21**, 423–446.

Waliser, D. E., R. Murtugudde, and L. Lucas, 2004: Indo-Pacific ocean response to atmospheric intraseasonal variability. Part II: Boreal summer and the intraseasonal oscillation. *J. Geophys. Res.*, **109**, C03 030, 10.1029/2003JC002 002.

Waliser, D. E., W. Stern, S. Schubert, and K. M. Lau, 2003b: Dynamic predictability of intraseasonal variability associated with the Asian summer monsoon. *Quart. J. Roy. Meteor. Soc.*, **129**, 2897–2925.

Wang, B., Q. Ding, X. Fu, I.-S. Kang, K. Jin, J. Shukla, and F. Doblas-Reyes, 2005: Fundamental challenge in simulation and prediction of summer monsoon rainfall. *Geophys. Res. Lett.*, **32**, L15 711, doi:10.1029/2005GL022 734.

Webster, P. J., E. F. Bradley, C. W. Fairall, J. S. Godfrey, P. Hacker, R. A. H. Jr., R. Lukas, Y. Seraa, J. M. Hummon, T. D. M. Lawrence, C. A. Russell, M. N. Ryan, K. Sahami, and P. Zuidema, 2002: The JASMINE pilot study. *Bull. Amer. Meteor. Soc.*, **83 (11)**, 1603–1630.

Webster, P. J. and C. Hoyos, 2004: Prediction of monsoon rainfall and river discharge on 15-30-day time scales. *Bull. Amer. Meteor. Soc.*, **85**, 1745–1767.

Wentz, F. J., C. Gentemann, D. Smith, and D. Chelton, 2000: Satellite measurements of sea surface temperature through clouds. *Science*, **288 (5467)**, 847–850.

Xavier, P. K. and B. N. Goswami, 2007: An analog method for real-time forecasting of summer monsoon sub-seasonal variability. *Mon. Wea. Rev.*, (in press).

Printed January 17, 2008.

Figure captions

1. Time-latitude section of the climatological (average of 22 years for observations and 9 members and 22 years for models) daily evolution of OLR average between 75°-105°E (Bay of Bengal) during the 180 days of hindcasts. Values are in W m^{-2}.

2. A demonstration of the construction of intraseasonal OLR anomalies. The dotted line in (a) shows the prefixed OLR data from ERA40 till 30 April and the hindcasts of SMPI model (starting from 1 May, indicated by the vertical black line) for the year 1995 at the location 95°E, 15°N. The thick solid line shows the daily climatologies of ERA40 and model that are removed from the data to yield daily values of anomalies (dotted line in b). This construction of daily anomalies reduces the jump at the beginning of the hindcasts. The thick solid line in (b) shows the 20-90 day bandpass filtered anomalies. All values are in W m^{-2}.

3. (a) Climatological values of intraseasonal (20-90 days filtered) standard deviation of OLR for the months of May, June and JAS (W m^{-2}). The 3 right panels (b) show the intraseasonal standard deviation of SWS (m s^{-1}) for May, June and JAS. 120 days of ERA40 anomalies have been prefixed to the hindcast anomalies before filtering to avoid loss of information in the first two months of hindcasts (May and June).

4. Same as Fig.3, but for the SST (K). The top panels are the ISV of SST from TMI for the period 1998-2004.

5. Climatological values of mixed layer depths (m) for the months of May, June and JAS from de Boyer Montegut et al. (2004) climatology (top panels), and from models. The mixed layer climatology of de Boyer Montegut et al. (2004) shown here is based on an optimal temperature criterion of 0.2°K absolute difference from surface.

6. The average patterns of local modes of OLR for May, June and JAS. The number of local modes used to construct each pattern is indicated on the top left of each panel. For

example, the observed May pattern is constructed from 16 events in the 21 years, while in the models it is constructed from patterns from 21 years and 9 ensemble members. The segment length is proportional to the standard deviation and the angle of the segments represents the relative phase. The angle increases clockwise with time (e.g. northward propagation for a segment rotating clockwise towards the north). Shades represent the standard deviation of these patterns in W m^{-2}.

7. Ratio of local mode amplitude to the 20-90 day amplitude of OLR from May-September from the observations and models. The value for a particular region represents the average contribution of large-scale organized convective perturbations to the local, more stochastic (or related to local instability) convective variability.

8. Monthly averages of period (days, (a)) and variance percentage of each local mode (b). (c) shows the normalized distance of individual local modes from the average summer mode averaged for each month. These values result from the average over 21 years in the case of observations and all the 21 years and 9 members for the hindcasts.

9. Distribution of distances between individual local modes and the average summer (May-September) mode of all models and observations.

10. Distribution of distances between local modes of each model to the average observed mode. Distributions are shown for May, June, JAS and May-September.

11. Phase difference between the SST perturbation and the OLR (the left panels), between SST perturbations and the surface wind speed (the middle panels) and between OLR and surface wind speed (the right panels) for the summer season. For the left figures a northward (eastward) pointer means that the OLR is minimal 1/4 period before (simultaneous with) the SST minimum. For middle panels, a southward (westward) pointer means that the surface wind speed is maximal 1/4 of the period before (simultaneous with) the minimum SST. For right panels, a southward (westward) pointer means that

the surface wind speed is maximal 1/4 of the period after (simultaneous with) the minimum. Segment length is proportional to the product of normalized standard deviations of both considered parameters.

12. Histogram of the phase differences between SST and OLR (a), SST and SWS (b) and OLR and SWS (c) over every grid points of the Bay of Bengal (80°-95°E, 5°-20°N). The full life cycle of one ISV event is taken as 2π radians. Values are binned for every $\pi/4$ radians. Frequency percentage for each bin is plotted at the centre of the bin.

13. A schematic of the observed and modeled phase relationships between OLR, SST and SWS. A full cycle of an ISV event is shown with normalized amplitudes. The phase differences are based on the medians of values presented in Fig.12.

14. The difference between ISV of OLR and SST for models with same OGCM (CRFC and LODY; a,c) and same AGCMs (LODY and SCWC; b,d). Units of OLR ISV is W m^{-2} and SST ISV is K.

Figure Captions

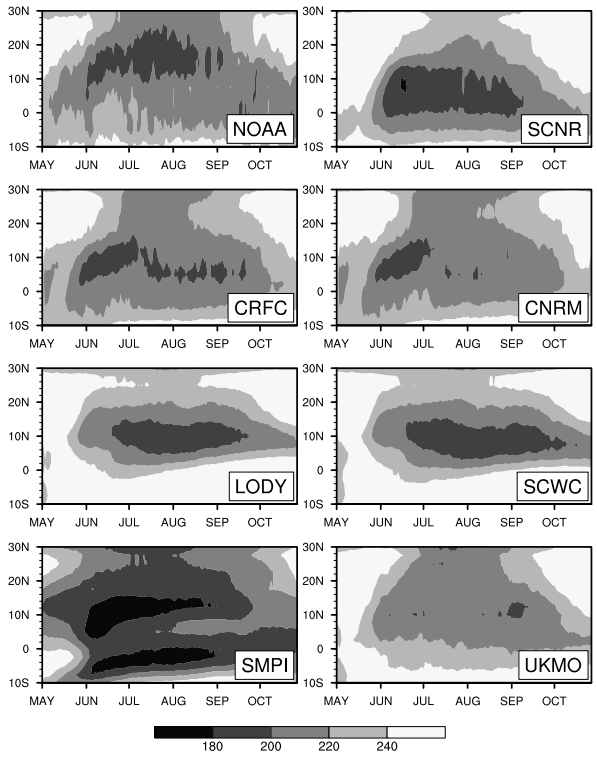

FIG. 1. Time-latitude section of the climatological (average of 22 years for observations and 9 members and 22 years for models) daily evolution of OLR average between 75°-105°E (Bay of Bengal) during the 180 days of hindcasts. Values are in W m^{-2}.

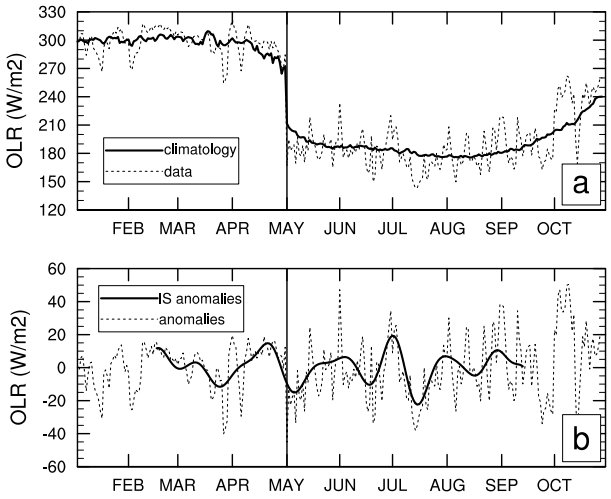

FIG. 2. A demonstration of the construction of intraseasonal OLR anomalies. The dotted line in (a) shows the prefixed OLR data from ERA40 till 30 April and the hindcasts of SMPI model (starting from 1 May, indicated by the vertical black line) for the year 1995 at the location 95°E, 15°N. The thick solid line shows the daily climatologies of ERA40 and model that are removed from the data to yield daily values of anomalies (dotted line in b). This construction of daily anomalies reduces the jump at the beginning of the hindcasts. The thick solid line in (b) shows the 20-90 day bandpass filtered anomalies. All values are in W m^{-2}.

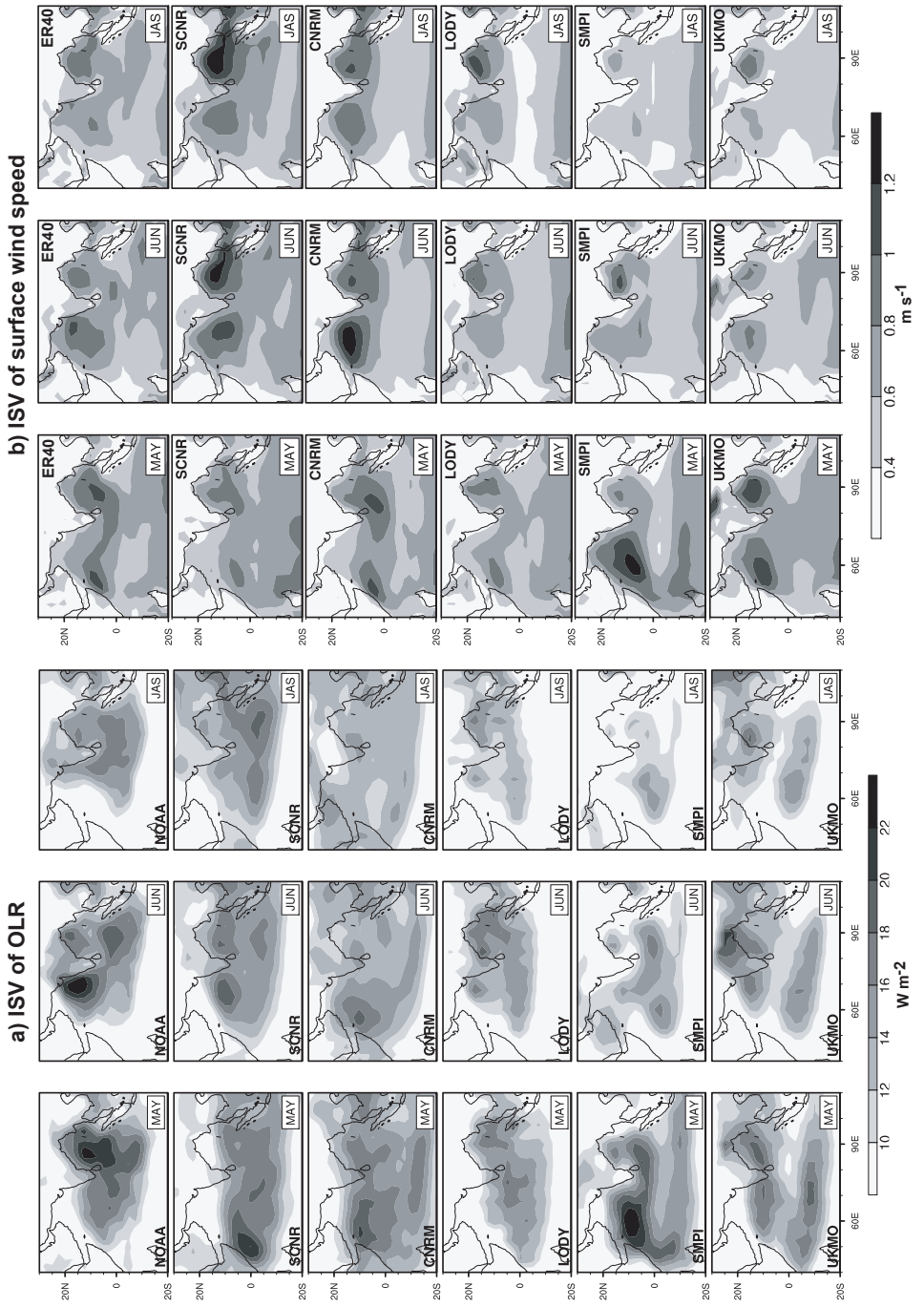

FIG. 3. (a) Climatological values of intraseasonal (20-90 days filtered) standard deviation of OLR for the months of May, June and JAS (W m^{-2}). The 3 right panels (b) show the intraseasonal standard deviation of SWS (m s^{-1}) for May, June and JAS. 120 days of ERA40 anomalies have been prefixed to the hindcast anomalies before filtering to avoid loss of information in the first two months of hindcasts (May and June).

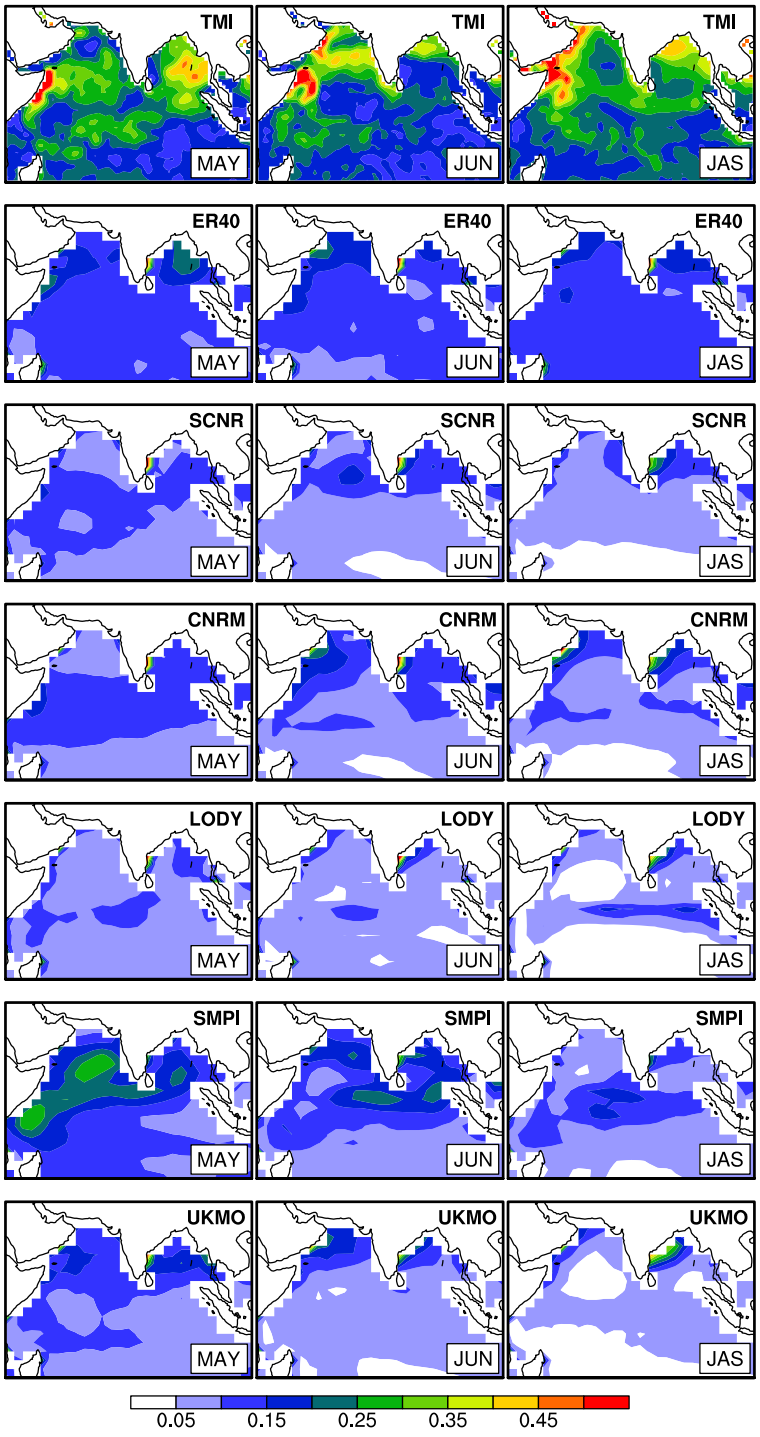

FIG. 4. Same as Fig.3, but for the SST (K). The top panels are the ISV of SST from TMI for the period 1998-2004.

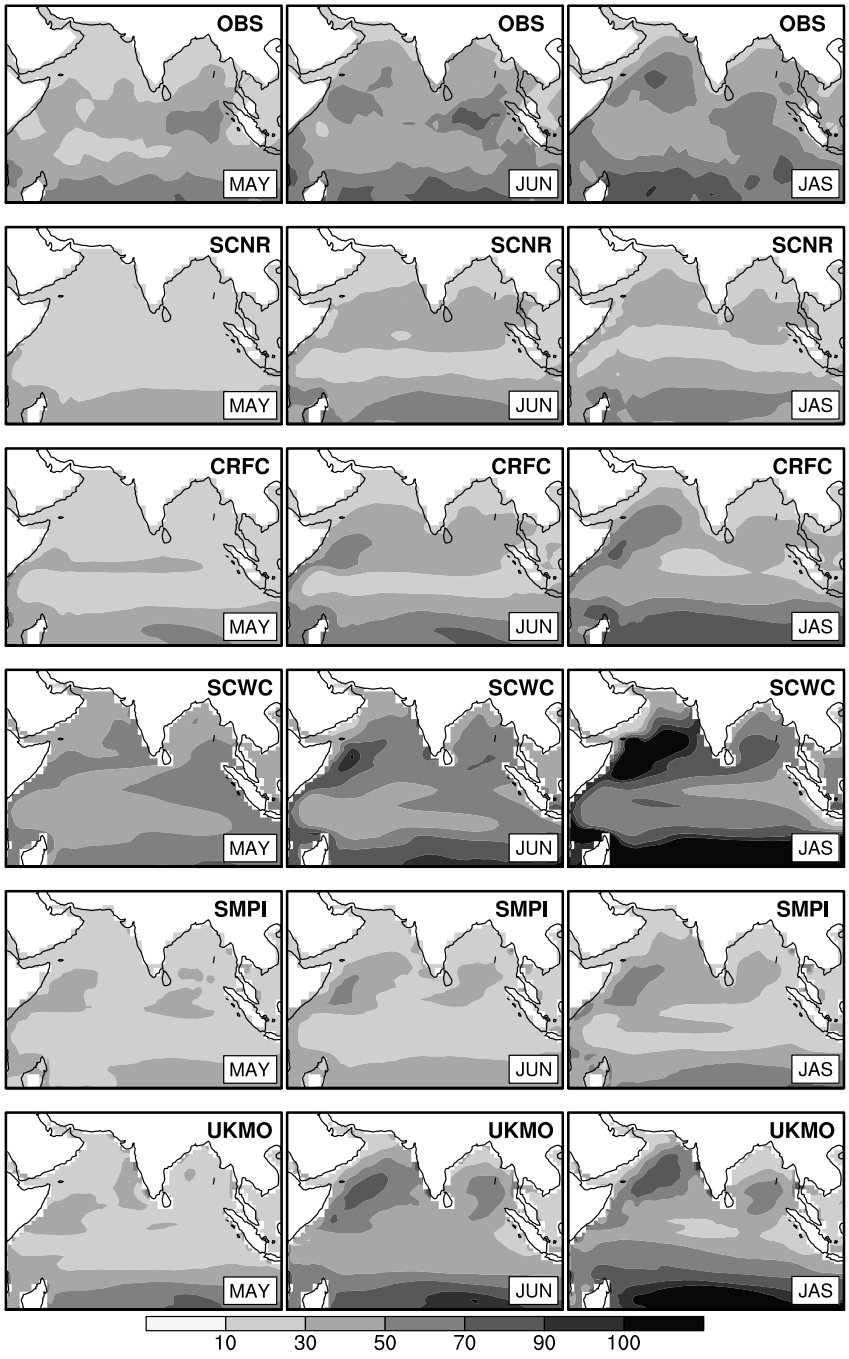

FIG. 5. Climatological values of mixed layer depths (m) for the months of May, June and JAS from de Boyer Montegut et al. (2004) climatology (top panels), and from models. The mixed layer climatology of de Boyer Montegut et al. (2004) shown here is based on an optimal temperature criterion of 0.2°K absolute difference from surface.

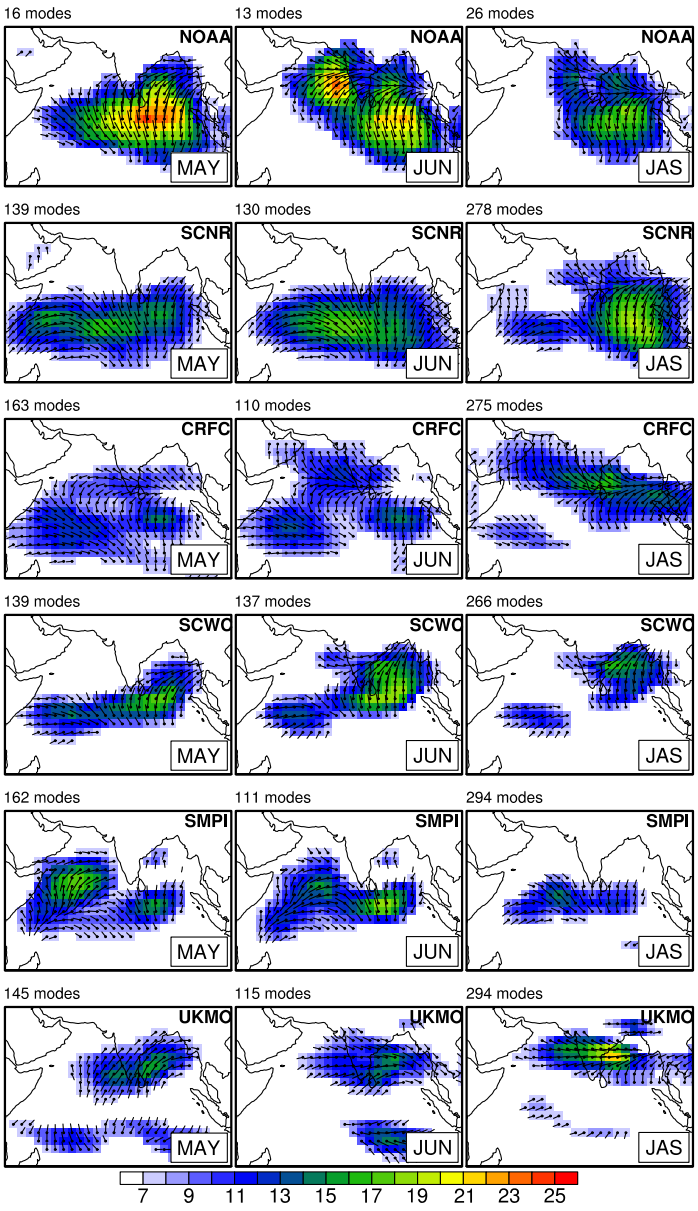

FIG. 6. The average patterns of local modes of OLR for May, June and JAS. The number of local modes used to construct each pattern is indicated on the top left of each panel. For example, the observed May pattern is constructed from 16 events in the 21 years, while in the models it is constructed from patterns from 21 years and 9 ensemble members. The segment length is proportional to the standard deviation and the angle of the segments represents the relative phase. The angle increases clockwise with time (e.g. northward propagation for a segment rotating clockwise towards the north). Shades represent the standard deviation of these patterns in W m^{-2}.

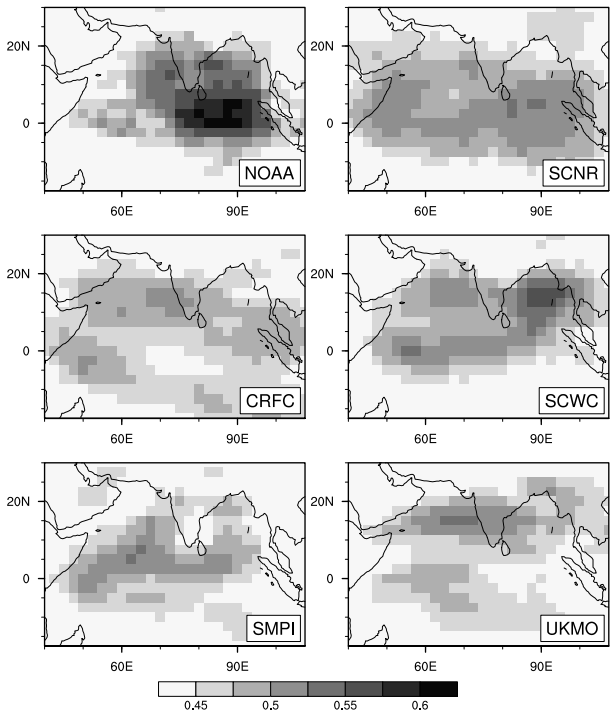

FIG. 7. Ratio of local mode amplitude to the 20-90 day amplitude of OLR from May-September from the observations and models. The value for a particular region represents the average contribution of large-scale organized convective perturbations to the local, more stochastic (or related to local instability) convective variability.

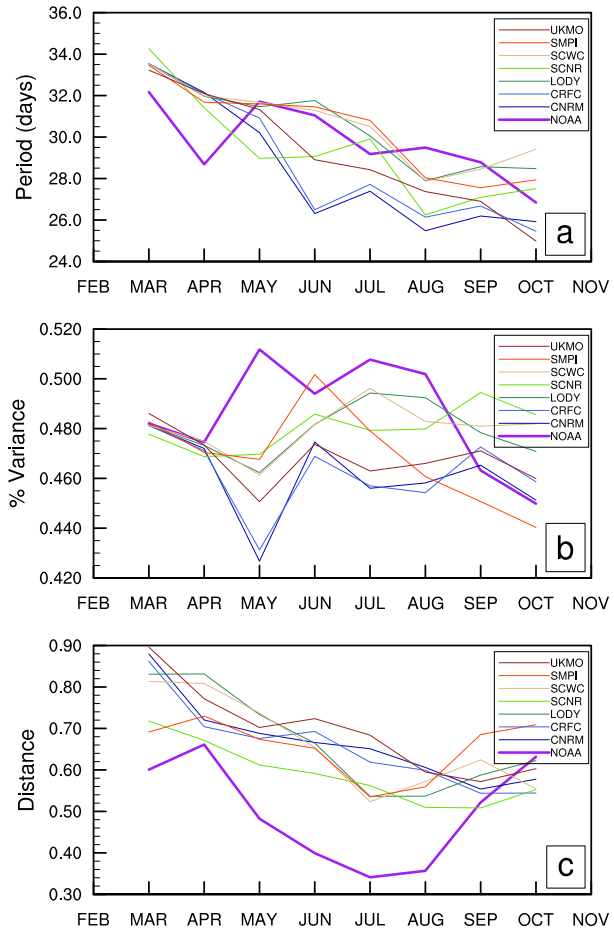

FIG. 8. Monthly averages of period (days, (a)) and variance percentage of each local mode (b). (c) shows the normalized distance of individual local modes from the average summer mode averaged for each month. These values result from the average over 21 years in the case of observations and all the 21 years and 9 members for the hindcasts.

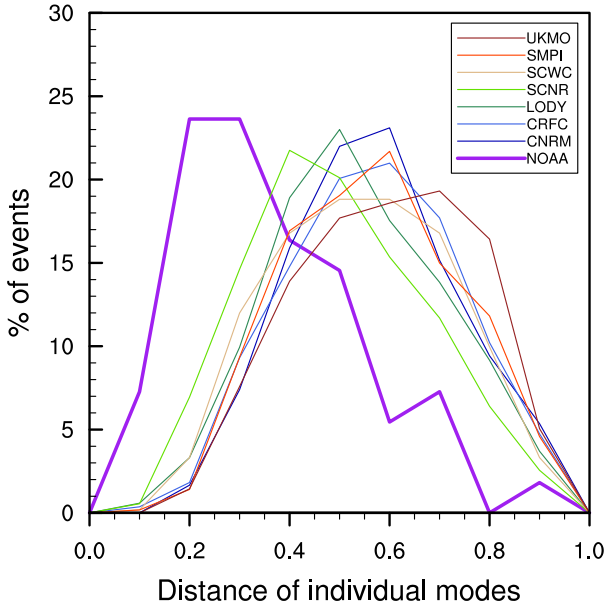

FIG. 9. Distribution of distances between individual local modes and the average summer (May-September) mode of all models and observations.

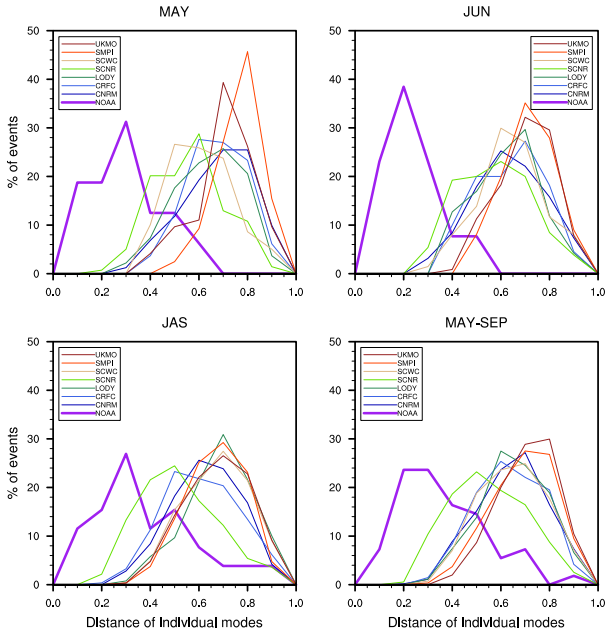

FIG. 10. Distribution of distances between local modes of each model to the average observed mode. Distributions are shown for May, June, JAS and May-September.

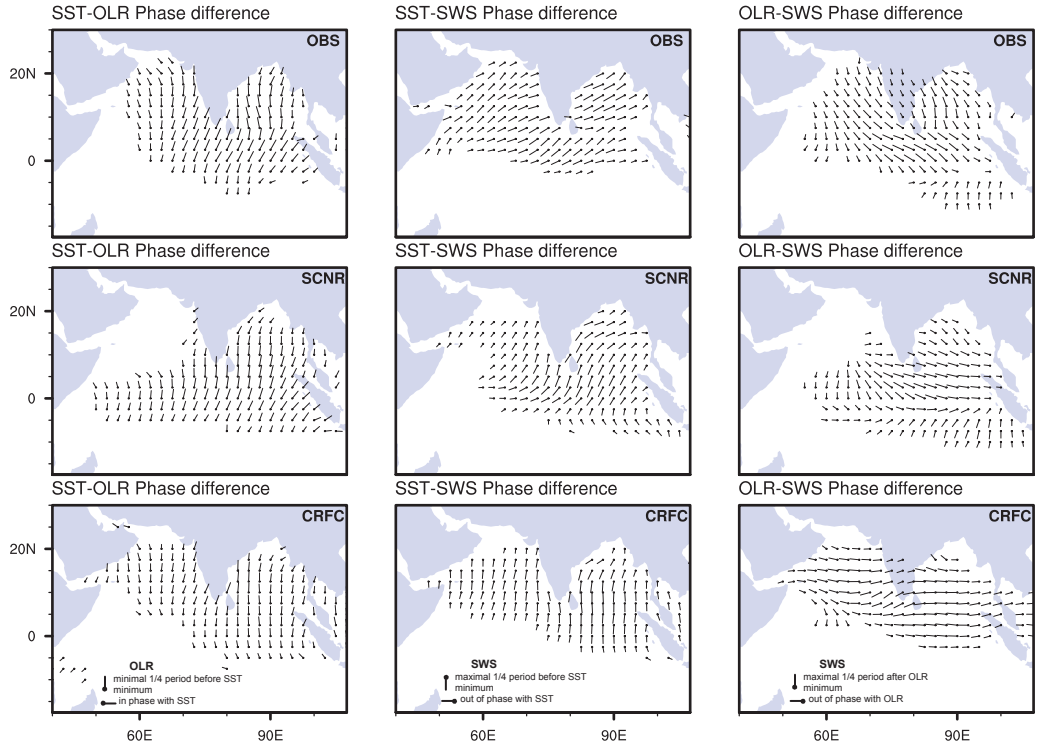

FIG. 11. Phase difference between the SST perturbation and the OLR (the left panels), between SST perturbations and the surface wind speed (the middle panels) and between OLR and surface wind speed (the right panels) for the summer season. For the left figures a northward (eastward) pointer means that the OLR is minimal 1/4 period before (simultaneous with) the SST minimum. For middle panels, a southward (westward) pointer means that the surface wind speed is maximal 1/4 of the period before (simultaneous with) the minimum SST. For right panels, a southward (westward) pointer means that the surface wind speed is maximal 1/4 of the period after (simultaneous with) the minimum. Segment length is proportional to the product of normalized standard deviations of both considered parameters.

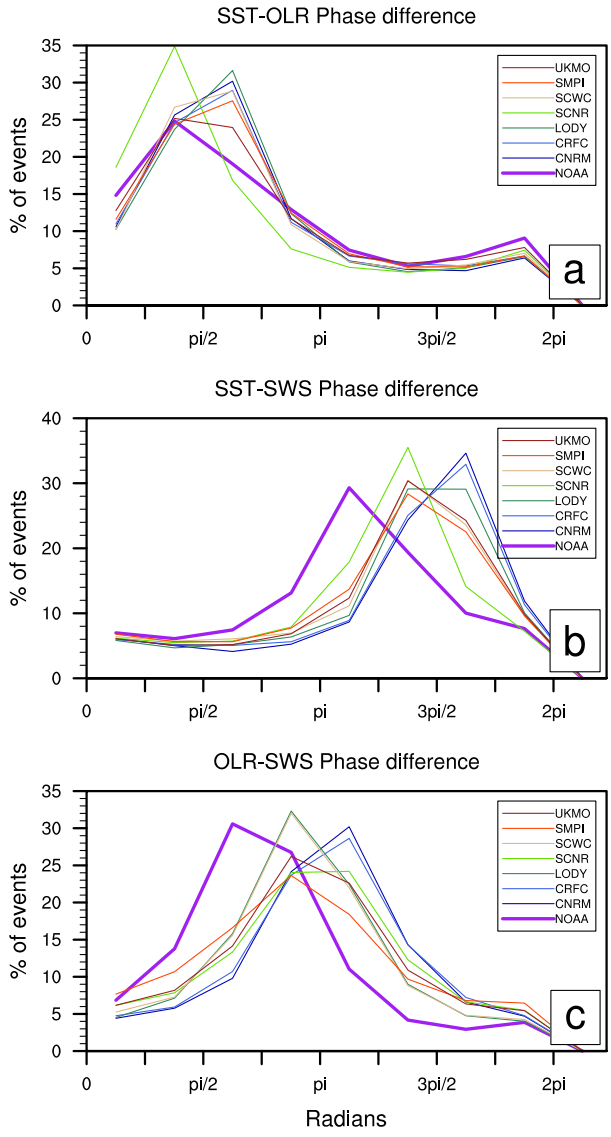

FIG. 12. Histogram of the phase differences between SST and OLR (a), SST and SWS (b) and OLR and SWS (c) over every grid points of the Bay of Bengal (80°-95°E, 5°-20°N). The full life cycle of one ISV event is taken as 2π radians. Values are binned for every $\pi/4$ radians. Frequency percentage for each bin is plotted at the centre of the bin.

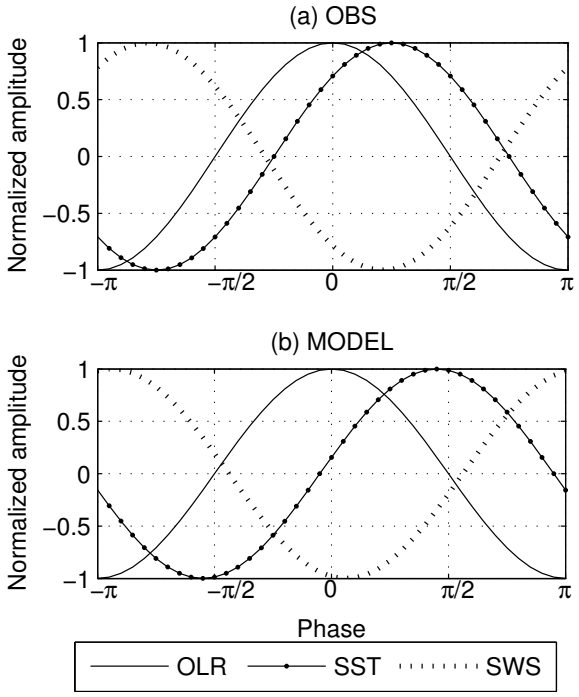

FIG. 13. A schematic of the observed and modeled phase relationships between OLR, SST and SWS. A full cycle of an ISV event is shown with normalized amplitudes. The phase differences are based on the medians of values presented in Fig.12.

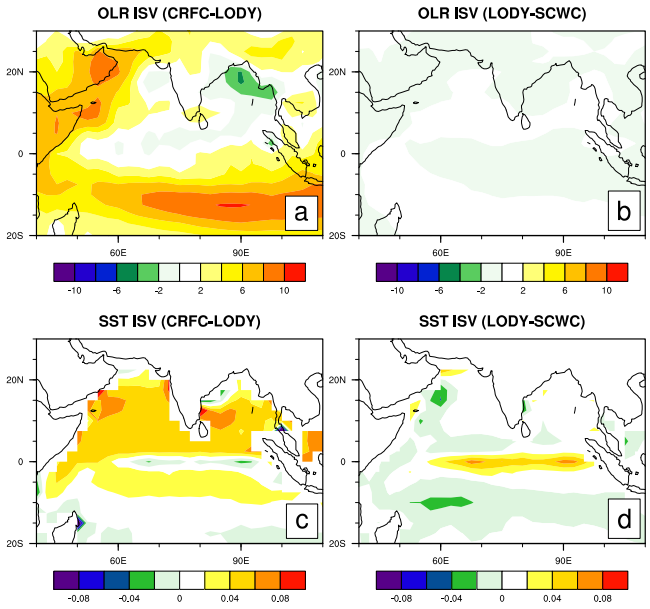

FIG. 14. The difference between ISV of OLR and SST for models with same OGCM (CRFC and LODY; a,c) and same AGCMs (LODY and SCWC; b,d). Units of OLR ISV is W m^{-2} and SST ISV is K.

Tables

Model	AGCM			OGCM		
Name	Model	Resolution	Initial Condition	Model	Resolution	Initial Condition
CNRM	ARPEGE	T63L31	ERA40	OPA8.1	2×1.5(0.5 Eq.) 31 levels	ERA40 forced ocean analysis
CRFC	ARPEGE	T63L31	ERA40	OPA8.2	2×2(0.5 Eq.) 31 levels	ERA40 forced ocean analysis
LODY	IFS	T95L40	ERA40	OPA8.2	2×2(0.5 Eq.) 31 levels	ERA40 forced ocean analysis
SCNR	ECHAM4	T42L19	Coupled AMIP type run	OPA8.1	2×1.5(0.5 Eq.) 31 levels	ERA40 forced ocean analysis
SCWC	IFS	T95L40	ERA40	HOPE-E	1.4×1.4(0.3 Eq.) 29 levels	ERA40 forced ocean analysis
SMPI	ECHAM5	T42L19	Coupled run relaxed to obs.SST	MPI-OM1	2.5×2.5(0.5 Eq.) 23 levels	Coupled run relaxed to obs.SST
UKMO	HadCM3	2.5×3.75 L19	ERA40	GloSea	1.25×1.25(0.3 Eq.) 40 levels	ERA40 forced ocean analysis

TABLE 1. Components of the seven comprehensive European global coupled atmosphere-ocean models are installed at European Centre for Medium-Range Weather Forecasts (ECMWF). They are abbreviated as CNRM (Centre National de Recherche en Meteorologie), CRFC (European Centre for Research and Advanced Training in Scientific Computation, France; CERFACS), LODY (Laboratoire d'Ocenographie Dynamique et de Climatologie, France; LODYC), SCNR (National Institute for Geophysics, Italy; INGV), SCWC (ECMWF), SMPI (Max-Planck Institute fur Meteorology, Germany; MPI) and UKMO (Meteorological Office, UK).